THE JOURNAL OF BIOLOGICAL CHEMISTRY VOL. 283, NO. 44, pp. 29993–30009, October 31, 2008

Analysis of a Membrane Interacting Region of Herpes Simplex Virus Type 1 Glycoprotein H*

Received for publication, April 22, 2008, and in revised form, July 23, 2008 Published, JBC Papers in Press, August 4, 2008, DOI 10.1074/jbc.M803092200

Stefania Galdiero[‡§¶], Annarita Falanga[‡], Mariateresa Vitiello[‖], Luca Raiola[**], Roberto Fattorusso[**], Helena Browne[‡‡], Carlo Pedone[‡§¶], Carla Isernia[**], and Massimiliano Galdiero[§‖1]

*From the [‖]Department of Experimental Medicine-II, University of Naples, Via De Crecchio 7, 80138, Napoli, Italy, [‡]Department of Biological Sciences, Division of Biostructures and [§]Centro Interuniversitario di Ricerca sui Peptidi Bioattivi, University of Naples "Federico II", Via Mezzocannone 16, 80134, Napoli, Italy, [¶]Istituto di Biostrutture e Bioimmagini, Consiglio Nazionale delle Ricerche, Via Mezzocannone 16, 80134, Napoli, Italy, [‡‡]Division of Virology, Department of Pathology, University of Cambridge, Cambridge CB2 1QPz, United Kingdom, and the **Department of Environmental Science-II, University of Naples, via Vivaldi 43, 81100 Caserta, Italy*

Glycoprotein H (gH) of herpes simplex virus type I (HSV-1) is involved in the complex mechanism of membrane fusion of the viral envelope with the host cell. Membrane interacting regions and potential fusion peptides have been identified in HSV-1 gH as well as glycoprotein B (gB). Because of the complex fusion mechanism of HSV-1, which requires four viral glycoproteins, and because there are only structural data for gB and glycoprotein D, many questions regarding the mechanism by which HSV-1 fuses its envelope with the host cell membrane remain unresolved. Previous studies have shown that peptides derived from certain regions of gH have the potential to interact with membranes, and based on these findings we have generated a set of peptides containing mutations in one of these domains, gH-(626–644), to investigate further the functional role of this region. Using a combination of biochemical, spectroscopic, and nuclear magnetic resonance techniques, we showed that the α-helical nature of this stretch of amino acids in gH is important for membrane interaction and that the aromatic residues, tryptophan and tyrosine, are critical for induction of fusion.

Herpes simplex virus (HSV),[2] the prototype of the alphaherpesviruses, is a human pathogen that infects epithelial cells before spreading to the peripheral nervous system to establish a life long latent infection. It is an enveloped DNA virus and needs to fuse its membrane with a cellular membrane to establish infection. Of the dozen or more envelope glycoproteins in the HSV virion, five have a role in viral entry (1). Glycoproteins gB and/or gC can mediate the binding of virus to cell surface heparan sulfate or related glycosaminoglycans (2), although the interaction of envelope glycoprotein gD with any one of several cell surface receptors is also needed to allow entry into susceptible cells. These molecules include the following: HVEM (3), a member of the tumor necrosis factor receptor family; nectin-1 (4) and nectin-2 (5), cell adhesion molecules belonging to the immunoglobulin superfamily; and specific sites in heparan sulfate generated by particular 3-*O*-sulfotransferases (6). The activation of the fusion machinery is dependent on the interaction of any of these receptors with gD, whose N-terminal conformational changes trigger the gB trimer and/or the heterodimer gH-gL (7–11), resulting in entry by envelope:membrane fusion. It has also been reported recently that gB associates with PILR-α, and this has been proposed as a further cellular receptor involved in HSV entry (12).

The minimal fusion machinery in HSV is composed of gD, gB, and gH/gL, which are all essential for the entry process (1, 13), and expression of this quartet of glycoproteins induces the fusion of cellular membranes in the absence of virus infection (14). This complexity is in contrast to most enveloped viruses, which generally require only 1 or 2 envelope proteins to mediate fusion (15). Of the four glycoproteins that are essential for HSV entry, gB and gH have both been proposed as candidates for direct induction of membrane fusion.

The fusogenic properties of gB are well established (1, 16, 17), and its structure displays features of both class I and class II membrane-fusion proteins (18). In fact, the crystal structure of HSV-1 gB (9) revealed an unexpected structural homology to the envelope glycoprotein of the vesicular stomatitis virus (19). These data allowed the identification of a putative fusion peptide in gB and suggested the identification of a third class of fusion proteins. Although no structural data for gH/gL from HSV-1 (or any of its homologues in other herpesviruses) are available, gH has also been considered as a likely fusion effector (20, 21).

HSV-1 gH is an 838-residue type 1 membrane glycoprotein. The ectodomain contains 7 *N*-glycosylation sites and 8 cysteine residues forming at least 2 disulfide bonds between cysteines 5 and 6 (residue 554 and 589) and cysteines 7 and 8 (residues 652 and 706) (22). The N- and C-terminal halves of gH include separate structural and functional segments (23, 24). The only function associated with the N-terminal domain is gL binding,

* The costs of publication of this article were defrayed in part by the payment of page charges. This article must therefore be hereby marked "*advertisement*" in accordance with 18 U.S.C. Section 1734 solely to indicate this fact.

[1] To whom correspondence should be addressed. Tel.: 39-081-5667646; Fax: 39-081-5667578; E-mail: massimiliano.galdiero@unina2.it.

[2] The abbreviations used are: HSV, herpes simplex virus; HSV-1, herpes simplex virus, type I; gH, glycoprotein H; DMEM, Dulbecco's modified Eagle's medium; PC, phosphatidylcholine; Chol, cholesterol; NBD, 4-chloro-7-nitrobenz-2-oxa-1,3-diazole; PE, phosphatidylethanolamine; LUV, large unilamellar vesicle; SUV, small unilamellar vesicle; gB, glycoprotein B; gL, glycoprotein L; TFE, trifluoroethanol; r.m.s.d., root mean square deviation; Fmoc, 9-fluorenylmethoxycarbonyl; TOCSY, total correlation spectroscopy; NOE, nuclear Overhauser effect; NOESY, nuclear Overhauser effect spectroscopy; ROESY, rotating frame nuclear Overhauser enhancement spectroscopy; ENZ, enzyme.

to form a noncovalently linked heterodimer. The formation of the heterodimer is strictly required for gH/gL maturation, transport, and incorporation into the virion particle (25, 26).

Several domains likely to be important for membrane fusion have been identified in the C-terminal region of gH. For example, certain mutations in the transmembrane region and cytoplasmic tail affect fusion (27, 28), as do mutations in the region preceding the transmembrane (24). Furthermore, peptides matching a number of regions of the gH ectodomain have been shown to interact with membranes and have been proposed to play a role in the fusion process (20, 21).

gH has been reported to have certain features that are characteristic of class I fusion proteins, such as the presence of heptad repeats and a putative fusion peptide region (21, 29, 30). Moreover, recent data have shown that peptides spanning the heptad-repeat region of gH inhibit the entry of both human cytomegalovirus (31) and HSV-1 (29, 30), similar to the corresponding entry inhibitors identified for viruses that have a class I membrane-fusion protein.

The physical event needed to promote membrane fusion induced by enveloped viruses is the insertion of the fusion peptide from one of the viral proteins into the cellular membrane to disrupt the normal organization of the lipids in their vicinity. Even though the exact mechanism of insertion of the fusion peptide into the target cell membrane is still unknown, several studies suggest that membranotropic regions could potentially cause the membrane distortion necessary for fusion in relation to their high propensity to partition into the membrane interface.

We have previously demonstrated that synthetic peptides modeled on HSV-1 gH (gH-(220–262), gH-(381–420), gH-(493–537), and gH-(626–644)) are able to induce rapid membrane fusion and act in a synergistic way. These regions, in conjunction with the membrane-proximal region (32) and the transmembrane anchor of the protein, seem to form a continuous tract of hydrophobic membrane interacting surfaces that could simultaneously destabilize viral and cellular opposing membranes at the point of fusion. According to recent studies, binding of gD to its receptor is followed by hemifusion carried out by gH/gL, and full fusion is completed by the interaction between gH/gL and gB that concurrently leads to complete bilayer merging (33, 34). In this scenario, gH would seem to play a role in both hemifusion and complete fusion; therefore, the identified membranotropic regions could act in concert or sequentially during either of these steps.

The stretch of gH comprising amino acids 626–644 (as determined using the hydrophobicity-at-interface scale of Wimley and White (35)) showed characteristics of particular interest. When gH-(626–644) is in helical conformation, the polar residues concentrate on one face of the helix, giving a amphiphilic character common to fusion peptides of most fusion glycoproteins of enveloped viruses. Moreover, a peptide modeled on this region is very effective in inducing lipid mixing of model membranes; it can induce 50% fusion at a low peptide/lipid ratio. Peptide gH-(626–644) also has the characteristics of a putative fusion peptide because it has the ability to adopt different conformations when challenged in different environments: TFE, aqueous solution, SDS, and phospholipid vesicles.

A determination of the structure of this domain and of the role of specific amino acids in this region might therefore shed further light on the function of gH in membrane fusion. We generated a set of synthetic gH-(626–644) peptides with mutations in most of the conserved residues, such as glycines, alanines, leucines, tyrosines, and tryptophans, and analyzed them utilizing a combination of biochemical and spectroscopic techniques and nuclear magnetic resonance. The results reported here suggest that this gH membrane-perturbing domain might interact with biological membranes, contributing to the merging of the viral envelope and the cellular membrane, and that its activity is directly dependent on the adoption of an α-helical three-dimensional structure and on the presence of aromatic residues.

EXPERIMENTAL PROCEDURES

Design of Mutations—Residues chosen for substitutions were selected to reduce the hydrophobicity of the fusion peptide, alter the chemical character of the amino acid side chain and the length of the side chain, or eliminate the charged character of the residue. Each residue was substituted with a serine, considering that alanines were not ideal substitutions because of their high presence in fusion peptides and considering the necessity of reducing the hydrophobicity of the peptide. Glycine 626 was also substituted with a hydrophobic residue with a side chain (valine). The Wimley-White hydrophobicity of the mutated peptides was compared with that of the native sequence (Table 1).

Peptide Synthesis—Peptides were synthesized using standard solid-phase 9-fluorenylmethoxycarbonyl (Fmoc) method as reported previously (20). All purified peptides were obtained with good yields (30–40%). Table 1 shows the sequences of all the synthesized peptides. Peptide stock solutions were prepared in 2% dimethyl sulfoxide (DMSO). A scrambled peptide of the native sequence was synthesized, namely SGYARFNLAIAARLLTHTW.

NBD Labeling of Peptides—Labeling was performed on resin-bound peptides as reported previously by Rapaport and Shai (36). Briefly, 30–70 mg of resin-bound peptide (10–25 μmol) was treated with piperidine in *N*,*N*-dimethylformamide to remove the Fmoc-protecting group of the N-terminal amino acid of the linked peptide. The resin-bound peptide was then reacted with 4-chloro-7-nitrobenz-2-oxa-1,3-diazole (NBD-Cl) in *N*,*N*-dimethylformamide (3–4 eq). After 24 h, the resin-bound peptides were washed thoroughly with methylene chloride, and the peptides were then cleaved from the resin and purified as reported previously for the nonlabeled peptides. Under these conditions, a major product was obtained, possessing an NBD moiety attached to the N-terminal amino group of the peptide. The identity of this compound was confirmed by liquid chromatography/mass spectrometry.

Lipid Mixing Assays—Membrane lipid mixing was monitored using the resonance energy transfer assay reported by Struck *et al.* (37). The assay is based on the dilution of the NBD-PE (donor) and rhodamine-PE (acceptor). Dilution because of membrane mixing results in an increase in NBD-PE fluorescence. Thus, we monitored the change in donor emission as aliquots of peptides were added to vesicles. Vesicles

containing 0.6 mol % of each probe were mixed with unlabeled vesicles at a 1:4 ratio (final lipid concentration, 0.1 mM). Small volumes of peptides in dimethyl sulfoxide (DMSO) were added; the final concentration of DMSO in the peptide solution was no higher than 2%. The NBD emission at 530 nm was followed with the excitation wavelength set at 465 nm. A cutoff filter at 515 nm was used between the sample and the emission monochromator to avoid scattering interferences. The fluorescence scale was calibrated such that the zero level corresponded to the initial residual fluorescence of the labeled vesicles, and the 100% value corresponding to complete mixing of all lipids in the system was set by the fluorescence intensity of vesicles upon the addition of Triton X-100 (0.05% v/v) at the same total lipid concentrations of the fusion assay. All fluorescence measurements were conducted in PC/Chol (1:1) LUVs. Lipid mixing experiments were repeated at least three times, and the results were averaged. Control experiments were performed using a scrambled peptide and DMSO.

Membrane Binding Experiments and Accessibility of Peptide to Proteolytic Cleavage—Changes in the fluorescence of NBD-labeled peptides were measured upon their binding to vesicles. SUVs were used in all the fluorometric experiments to minimize differential light scattering effects (38). Lipid vesicles were added to a solution containing 0.1 μM NBD-labeled peptides in 5 mM Hepes, pH 7.4. Emission spectra were recorded at 530 nm before and after the addition of vesicles, with the excitation set at 467 nm (10 nm slit). All the fluorescence measurements were done on a Varian spectrofluorometer.

The degree of peptide association with lipid vesicles was measured by adding lipid vesicles to 0.1 μM NBD-labeled peptides, and the fluorescence intensity was measured as a function of the lipid/peptide molar ratio, with excitation set at 468 nm, and emission was set at 530 nm in three to four separate experiments. The lipid/peptide molar ratio was 3000:1 so that spectral contributions of the free peptide would be negligible. A control experiment was performed by titrating unlabeled peptides with lipids up to the maximal concentration used in the assay. The fluorescence values were corrected by taking into account the dilution factor corresponding to the addition of microliter amounts of liposomes and by subtracting the corresponding blank.

The protease cleavage experiment was performed under similar experimental conditions. Proteinase K (30 μg/ml) was added to vesicles loaded with NBD-labeled peptides to investigate the extent of protection from enzyme action by the membrane on each of the peptides tested, and fluorescence was measured with time. The peptide/lipid molar ratio was kept at a level such that all the peptide was assumed to bind to the vesicles. The net retention of fluorescence is attributed to the protection of peptide from protease cleavage. To estimate the percent of cleavage, a control experiment was done, in which the peptides were preincubated with the same amount of protease before the addition of phospholipids. The emission at the end of the control experiment was referred to as 100% cleavage.

Tryptophan Fluorescence Measurements—Tryptophan fluorescence increases with the increase in the environment hydrophobicity, and a blue shift of the emission maxima is observed. Emission spectra of the peptides (4 μM) containing the tryptophan residue in the absence or presence of target vesicles (PC/Chol = 1:1) were recorded between 300 and 400 nm with an excitation wavelength of 295 nm. Trp fluorescence measurements were done in the absence and presence of iodide, which acts as an aqueous collisional quencher.

The degree of peptide association with lipid vesicles was measured by adding lipid vesicles to 4 μM peptides, and the fluorescence intensity was measured as a function of the lipid/peptide molar ratio, in three to four separate experiments. The fluorescence values were corrected by taking into account the dilution factor corresponding to the addition of microliter amounts of liposomes and by subtracting the corresponding blank. The lipid/peptide molar ratio was 300:1.

Theoretical Model—The binding of hydrophobic peptides to membranes can be described as a partition equilibrium: $X_b = K_p C_f$, where K_p is the apparent partition coefficient in units of M^{-1}, X_b is the molar ratio of bound peptide per total lipid, and C_f is the equilibrium concentration of the free peptide in solution. To calculate X_b, we estimated F_∞, the fluorescence signal obtained when all the peptide is lipid-bound, either from the plateau region of the titration curve or from a double-reciprocal plot of F (total peptide fluorescence) *versus* C_L (total concentration of lipids), as suggested previously by Schwarz *et al.* (39). (F_∞ was obtained by extrapolation of a double-reciprocal plot of the total peptide fluorescence *versus* the total lipid concentration in the outer leaflet, *i.e.* $1/F$ *versus* $1/0.6\ C_L$). Knowing the fluorescence intensities of the free and bound forms of the peptide, the fraction of membrane-bound peptide, f_b, could be determined by the formula $f_b = (F - F_0)/(F_\infty - F_0)$, where F represents the fluorescence of peptide after the addition of the vesicles, and F_0 represents the fluorescence of the unbound peptide. Determining the value of f_b in turn allows us to calculate the equilibrium concentration of free peptide in the solution, C_f, as well as the extent of peptide binding X_b. It was assumed that the peptides were initially partitioned only over the outer leaflet of the SUV (60% the total lipid) (40). Therefore, values of X_b were corrected as follows: $X_b^* = X_b/0.6$.

The curve resulting from plotting X_b^* *versus* the concentration of the free peptide, C_f, is referred to as the conventional binding peptide isotherm. Plots of X_b^* *versus* C_f yield straight lines with the slope corresponding to K_p if a simple partition equilibrium is observed. However, when the binding isotherms are not straight lines, but deviate to increased binding at higher peptide concentrations, such a deviation is expected for the cooperative binding of peptides that self-associate at the membrane surface. If enough data points of C_f could be collected at very low free peptide concentrations, the surface partition coefficients, K_p, could be estimated from the initial slopes of the curves.

Quenching of Tryptophan Emission by Acrylamide—Aliquots of a 4 M solution of this water-soluble quencher were added to the peptide in the absence or presence of liposomes. Fluorescence was measured at an excitation wavelength of 295 nm, to reduce acrylamide absorbance (and the resulting inner filter effect), and emission at a wavelength of 340 nm, to eliminate interference from the Raman band of water (41). The data were analyzed according to the Stern-Volmer equation (42), $F_0/F = 1 + K_{sv}[Q]$, where F_0 and F represent the fluorescence intensities

in the absence and the presence of the quencher (Q), respectively, and K_{sv} is the Stern-Volmer quenching constant, which is a measure of the accessibility of tryptophan to acrylamide. Considering that acrylamide does not significantly partition into the membrane bilayer (41), the value for K_{sv} can be considered to be a reliable reflection of the bimolecular rate constant for collisional quenching of the tryptophan residue present in the aqueous phase. Accordingly, K_{sv} is determined by the amount of nonvesicle-associated free peptide as well as the fraction of the peptide residing in the surface of the bilayer.

Circular Dichroism Measurements—CD spectra were recorded using a Jasco J-715 spectropolarimeter in a 1.0-cm quartz cell at room temperature. Solutions of peptides (8 μM) were prepared in buffer and in trifluoroethanol (TFE) (a solvent widely used in CD on peptides for its properties to unmask helical propensities of hydrophobic residues) at 20, 40, and 80%. Peptide samples in SDS were prepared using the following protocol (43). All peptides were first dissolved in TFE. Immediately after preparation, the peptide solution was added to an equal volume of an aqueous solution containing the appropriate SDS concentration, and water was added to yield a 16:1 ratio of water to TFE by volume. The samples were vortexed and lyophilized overnight. The dry samples were rehydrated with deionized water to yield final SDS concentrations of 10 mM.

The spectra are an average of three consecutive scans from 260 to 195 nm and were recorded with a bandwidth of 3 nm, a time constant of 16 s, and a scan rate of 10 nm/min. Spectra were recorded and corrected for the blank. Mean residue ellipticities were calculated using the equation Obsd/*lcn,* where Obsd is the ellipticities measured in millidegrees; l is the length of the cell in centimeters; c is the peptide concentration in mol/liter, and n is the number of amino acid residues in the peptide.

NMR Measurements—All the experiments were carried out at 500 MHz on a Varian Unity 500 spectrometer. Spectra were processed using the Varian VnmrJ and XEASY (44) software. Sample solutions (about 2 mM) were prepared in TFE-d_3/H_2O (80:20 v/v) with deuterated D_2O (99.9% relative isotopic abundance) and TFE-d_3 (99%) purchased from Cambridge Isotope Laboratories. Chemical shifts were referenced to the residual methylene resonance of CF_3CD_2OD at 3.88 ppm. Mono-dimensional and two-dimensional spectra were collected at 300 K using a spectral width of 6000 Hz and the DPFGSE sequence (45) for the water suppression. Two-dimensional experiments DQFCOSY, TOCSY, ROESY, and NOESY (46) were recorded in the phase-sensitive mode using the States-Haberkorn method; mixing times used for TOCSY, NOESY, and ROESY experiments were 70, 250, and 150 ms, respectively. Typically, 64 transients of 4K data points were collected for each of the 256 increments; the data were zero filled to 1K in ω1. Squared shifted sine-bell functions were applied in both dimensions prior to Fourier transformation and base-line correction.

Structure Calculations—Experimental distance restraints for structure calculation were derived from the cross-peak volumes in NOESY spectra, recorded in TFE/H_2O (80:20 v/v). The NOESY cross-peaks were manually integrated using the XEASY software and converted to upper distance constraints according to an inverse sixth power peak volume-to-distance relationship for the backbone and to an inverse fourth power function for side chains, by using the CALIBA module of the CYANA program (47). Distance constraints together with the obtained scalar coupling constants were then used by the GRIDSEARCH module, implemented in CYANA, to generate a set of allowable dihedral angles. Structure calculation, which used the torsion angle dynamics protocol of CYANA, was then started from 100 randomized conformers. The 20 conformers with the lowest CYANA target function were further refined *in vacuo* by means of unrestrained energy minimization, using the Discover module of the Insight II software (Accelrys, Inc.). Several cycles of steepest descent were repeated until the energy difference between two successive steps was less than 10^{-3} kJ mol^{-1}. The structure analysis was performed with the program MOLMOL (48).

TABLE 1
Peptide sequences

	Sequence	Hydrophobicity
gH-(626–644)	GLASTLTRWAHYNALIRAF	2.6
G626S	SLASTLTRWAHYNALIRAF	2.30
G626V	VLASTLTRWAHYNALIRAF	2.54
L627S	GSASTLTRWAHYNALIRAF	1.91
L631S	GLASTSTRWAHYNALIRAF	1.91
W634S	GLASTLTRSAHYNALIRAF	0.62
Y637S	GLASTLTRWAHSNALIRAF	1.53
R642S	GLASTLTRWAHYNALISAF	3.28

Virus Entry Assays—Vero cells were grown in Dulbecco's modified Eagle's medium (DMEM) supplemented with 10% fetal calf serum. HSV-1 expressing β-galactosidase driven by the cytomegalovirus IE-1 promoter was propagated as described previously (13).

Peptides were dissolved in DMEM without serum and used at a range of concentrations. All experiments were conducted in parallel with scrambled peptides and no-peptide controls.

To assess the effect of peptides on inhibition of HSV infectivity, cells were incubated with increasing concentrations of peptide (10, 25, 50, and 100 μM) in the presence of serial dilutions of viral inoculum for 45 min at 37 °C. Nonpenetrated viruses were inactivated by citrate buffer (pH 3.0) after the 45-min incubation at 37 °C. Monolayers were incubated for 48 h at 37 °C in DMEM supplemented with carboxymethylcellulose, fixed, and stained with 5-bromo-4-chloro-3-indolyl-β-D-galactopyranoside (X-gal), and plaque numbers were scored. Experiments were performed in triplicate, and the percentage of inhibition was calculated with respect to no-peptide control experiments.

Toxicity—Peptide cytotoxicity was measured by a lactate dehydrogenase assay and was carried out according to manufacturer's instructions using a cytotoxicity detection kit (Roche Diagnostics).

RESULTS

Design of Mutations—The mutated peptides were designed based on criteria described under "Experimental Procedures" and are summarized in Table 1. Hydrophobicity analysis revealed that most of the peptides have a lower hydrophobicity at the interface compared with the native sequence (Table 1). Peptide R642S has a higher hydrophobicity profile, but this mutant was designed not to reduce hydrophobicity but to

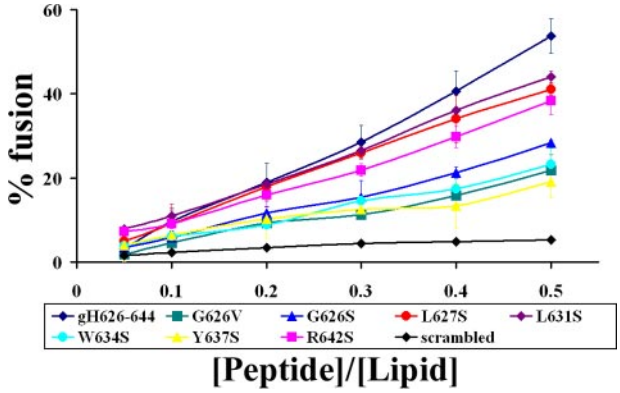

FIGURE 1. **Peptide-promoted membrane fusion of PC/Chol (1:1) LUVs as determined by lipid mixing; peptide aliquots were added to 0.1 mM LUVs, containing 0.6% NBD and 0.6% rhodamine.** The increase in fluorescence was measured after the addition of peptide aliquots; reduced Triton-X-100 (0.05% v/v) was referred to as 100% of fusion. In figure is reported the dose dependence of lipid mixing.

investigate the role of the charged side chain on membrane interaction and fusion (Table 1).

Ability of Mutated Peptides to Induce Lipid Mixing—To investigate the fusogenicity of wild type and mutated peptides, NBD and rhodamine-labeled PE were used as the donor and acceptor of fluorescence energy transfer. A population of LUVs labeled with both was mixed with a population of unlabeled LUVs, and increasing amounts of peptides were added. Dilution of the fluorescent-labeled vesicles via membrane fusion induced by the peptide results in a reduction in the fluorescence energy transfer efficiency, hence dequenching of the donor fluorescence. The dependence of the extent of lipid mixing on the peptide to lipid molar ratio was analyzed; increasing amounts of each peptide were added to a fixed amount of vesicles. To compare the activity of the different peptides, the percentage of lipid mixing as a function of the peptide to lipid molar ratio was calculated. Fig. 1 shows the results of lipid mixing assays in PC/Chol for gH-(626–644) and mutant peptides. All the mutant peptides induced lower levels of fusion compared with gH-(626–644). Peptides Y637S, W634S, G626S, and G626V showed a significantly lower percentage of fusion. The peptides Y637S and W634S were the least effective inducers of lipid mixing, suggesting that these aromatic residues (Tyr and Trp) may play a fundamental role in fusion. In G626V and G626S, the glycine at the N terminus of gH-(626–644) was substituted with either valine or serine, respectively. The serine substitution retained a certain level of fusogenity, whereas the valine substitution induced a significant loss of activity. The peptide R642S is also significantly impaired in its ability to cause fusion suggesting that the charged residue at the C terminus is important for the localization of the peptide inside the lipid bilayer. However, we observed a reduced, but still significant, induction of fusion by peptides L631S and L627S, indicating that the substitution of the two leucines with serines is not sufficient to abolish the fusion activity of the peptide. No significant levels of fusion were observed with the scrambled version of gH-(626–644).

Binding of gH-(626–644)-derived Peptides to Membranes—The NBD fluorescence is very sensitive to the dielectric constant of its environment and can be monitored in membrane binding studies (49, 50). We labeled all the mutant peptides and gH-(626–644) at the N terminus with NBD. NBD itself is a relatively small amphipathic fluorescent probe that does not significantly affect the partition behavior of the labeled peptides. Fluorescent emission spectra of peptides in Hepes buffer and in presence of PC/Chol (1:1) were obtained; spectra in buffer and in liposomes for gH-(626–644) and Y637S are shown in Fig. 2*A*. All the peptides in buffer exhibited an emission maximum around 550 nm, similar to the spectrum of the NBD moiety dissolved in water (49, 50). As they bind to the lipid bilayer, they all exhibit similar blue shifts and fluorescence enhancement; in particular, the fluorescence intensity dramatically increased, and the fluorescence maximum decreased to around 520 nm, indicating that they all retained the ability to bind to liposomal membranes. In these experiments the lipid/peptide molar ratio was consistently maintained at an elevated level (3000:1) so that spectral contributions of the free peptide would be negligible. These changes reflect the translocation of the NBD group to the lipid bilayer interface; no such changes could be detected using the control molecules NBD-Cl or NBD-PE. Blue shifts of this magnitude have been observed by others when surface-active NBD-labeled peptides interact with lipid membranes (36, 51, 52) and are consistent with the NBD probe located within or on the surface of the membrane.

The location of NBD inside the membrane is not sufficient evidence to support the view that the entire peptide is located within the bilayer. Thus, to determine whether the peptides are exposed to the aqueous phase in their membrane-bound state, NBD-labeled peptides were treated with the proteolytic enzyme proteinase K before and after binding to phospholipid membranes. All peptides were first analyzed in buffer (P + buffer), followed by the addition of SUVs (P + SUV), which for membrane penetrating peptides is supposed to cause an increase in fluorescence. Once the curve reached a plateau, indicating complete binding of NBD-labeled peptides to the membrane, proteinase K was added (P + SUV + ENZ) to the peptide-lipid complex. A decrease in fluorescence would indicate that the labeled peptides are exposed to the aqueous phase and are susceptible to degradation in their membrane-bound state; a constant value or an increase would indicate protection from enzymatic digestion. When the peptide is initially incubated with proteinase K, prior to the addition of lipid vesicles (P + ENZ), it is digested by the protease and a decrease in fluorescence should occur only if an aggregated NBD-labeled peptide is dissociated. When vesicles are added (P + ENZ + SUV) to degraded peptides, a small increase of fluorescence is observed because of the binding of partially uncleaved peptides to vesicles.

Fig. 3 shows the results from analyzing a fresh preparation of peptide gH-(626–644) (Fig. 3*A*) or following 24 h of solubilization in buffer (Fig. 3*B*). The fresh preparation of the NBD-labeled peptide was first observed in buffer (P + buffer), followed by the addition of SUVs (P + SUV), which caused a large increase in fluorescence, and finally by the addition of proteinase K (P + SUV + ENZ) to the peptide-lipid complex, which still caused another small increase of fluorescence, indicating that the peptide is protected against enzymatic digestion. When the peptide was initially incubated with proteinase K,

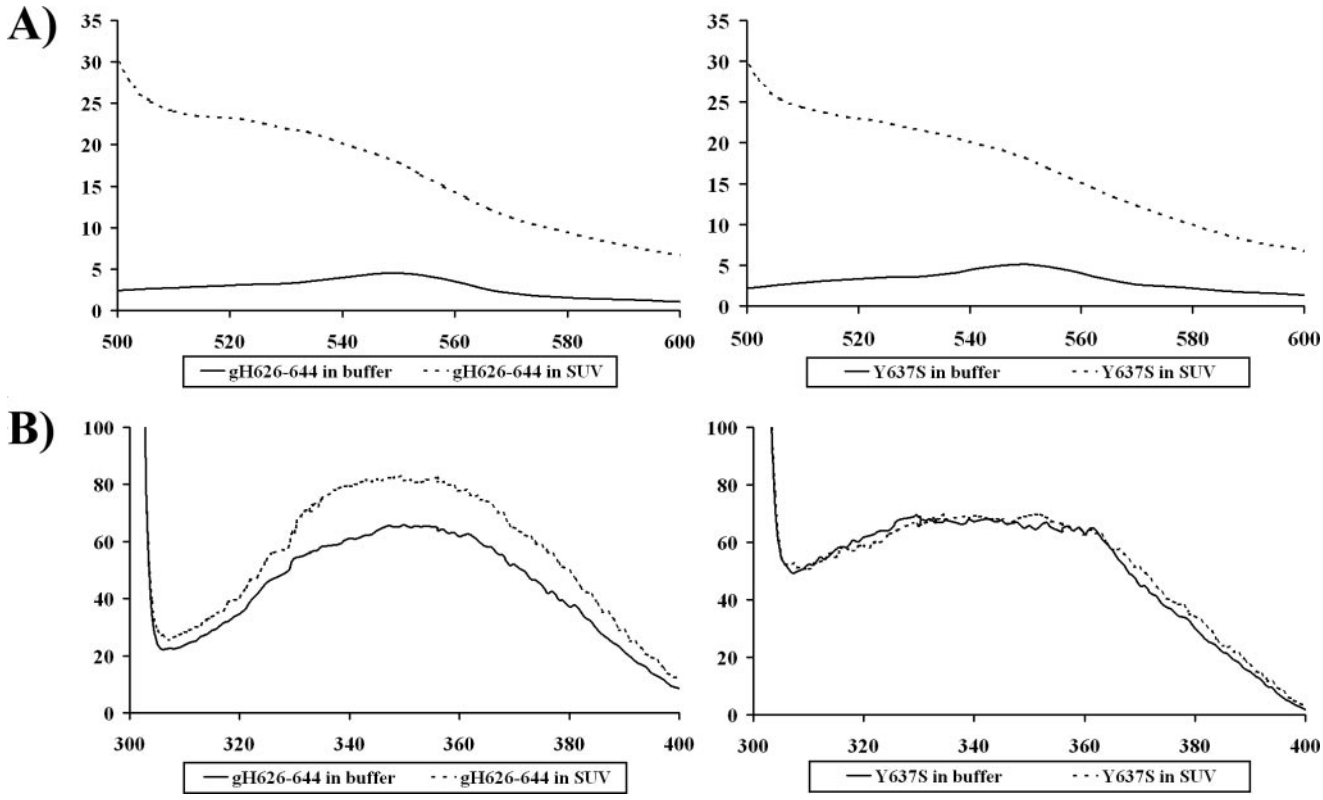

FIGURE 2. *A,* fluorescence spectra in buffer and in liposomes for gH-(626–644) and Y637S labeled with NBD. *B,* tryptophan fluorescence spectra in buffer and in liposomes for gH-(626–644) and Y637S.

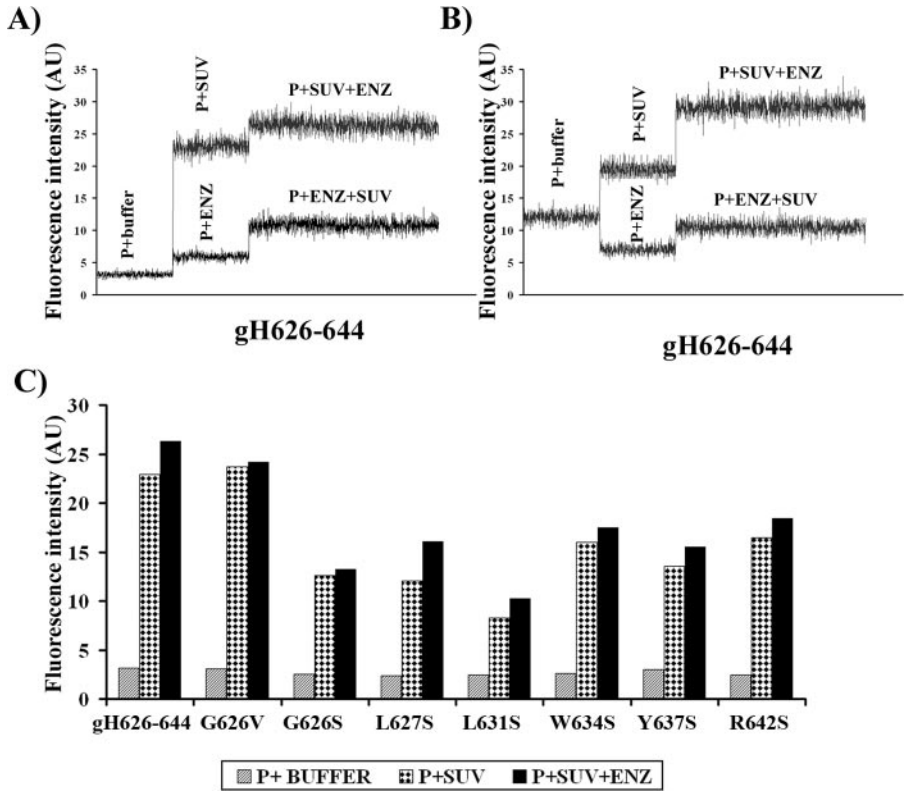

FIGURE 3. **Proteolytic digestion of membrane-bound NBD-labeled peptides.** The fluorescence emission spectra of the NBD-labeled peptide was monitored at 530 nm with excitation set at 467 nm. *A,* fresh preparation of the peptide gH-(626–644); *B,* peptide gH-(626–644) after 24 h from solubilization in buffer; *C,* results obtained for all the labeled peptides. *AU*, absorbance unit.

prior to the addition of lipid vesicles (P + ENZ), the peptide was digested by the protease (Fig. 3*A*). When vesicles were added (P + ENZ + SUV) to degraded peptides, a small increase of fluorescence was still observed, because of the binding of partially uncleaved peptides to vesicles. When the same experiment was performed on a preparation that had been solubilized for 24 h (Fig. 3*B*), the initial fluorescence value of the peptide in buffer was higher. This result is compatible with oligomerization of the peptide in buffer; the fluorescence values for P + SUV show that binding to the SUVs was comparable with that obtained for a fresh solution, indicating that the peptide in both the fresh solution and when oligomerized equally penetrates into the membrane. When the oligomerized peptide was initially incubated with proteinase K, prior to the addition of lipid vesicles (P + ENZ), the peptide was digested by the protease (Fig. 3*B*); we observed a decrease of fluorescence suggesting that the peptide is partially aggregated in buffer. When vesicles were added (P + ENZ + SUV) to

degraded peptides, a small increase of fluorescence was still observed because of the binding of partially uncleaved peptides to vesicles.

All other mutated peptides were subjected to a similar analysis (Fig. 3*C*). At the lipid/peptide molar ratios tested, most of the peptides bound to the vesicles, as indicated by the data in the P + SUV columns. The kinetics of binding for all the peptides were similar (data not shown). Fig. 3*C* shows that after proteinase K treatment, the fluorescence of all the NBD-labeled peptide increased. These results show that when the peptides are bound to phospholipid membranes they cannot be digested by proteinase K, suggesting that they are embedded within the phospholipid bilayer or, as result of conformational changes in their membrane-bound state, are less available for proteolysis. gH-(626–644), R642S, and G626S should be digested to similar extents by the protease and thus should have the same profile, but it is evident that gH-(626–644) penetrates more efficiently into the bilayer, indicating that the two residues mutated (arginine in R642S and glycine in G626S) may play a fundamental role in membrane interaction. It is also interesting to compare the results obtained for G626V and G626S; G626V, which has a hydrophobic residue instead of the glycine, is more efficient than G626S at penetrating the bilayer. All the other peptides analyzed penetrated less well into the bilayer. For comparison, proteinase K was added to a mixture of lipid vesicles and NBD-scrambled gH-(626–644), and no change in the fluorescence intensity occurred (data not shown).

Tryptophan Fluorescence Emission Analysis of Mutated Peptides—To extend the lipid mixing and protease protection experiments described above, we also measured the intrinsic fluorescence of the peptides (because of the presence of a tryptophan residue in the middle of the sequence) to evaluate the degree of penetration of the peptides into the membrane bilayer. We compared the fluorescence emission spectra of all the peptides containing the tryptophan in the presence of PC/Chol vesicles with that in buffer. Spectra in buffer and in liposomes for gH-(626–644) and Y637S are shown in Fig. 2*B*. The fluorescence emission of tryptophan residues increases when the amino acid enters a more hydrophobic environment, and together with an increase in quantum yield, the maximal spectral position is shifted toward shorter wavelengths (blue shift). For peptides gH-(626–644), L631S and L627S changes in the spectral properties were observed, suggesting that the single tryptophan residue of each peptide is located in a less polar environment upon interaction with lipids. Emission intensity was enhanced and the maxima shifted to lower wavelength; blue shifts of this magnitude have been observed when amphiphilic tryptophan-containing peptides interact with phospholipid bilayers (53) and are consistent with the indole moiety becoming partially immersed in the membrane (53), further suggesting that the peptides are capable of penetrating a lipid bilayer. The peptide R642S presents a spectrum that is compatible with a reduced ability to penetrate the bilayer, indicating that the arginine residue at the C terminus may be important for the positioning of the peptide inside the membrane. No significant changes of spectra were observed for G626V and G626S, suggesting that these peptides are unable to penetrate into the lipid bilayer. Because both G626S and G626V

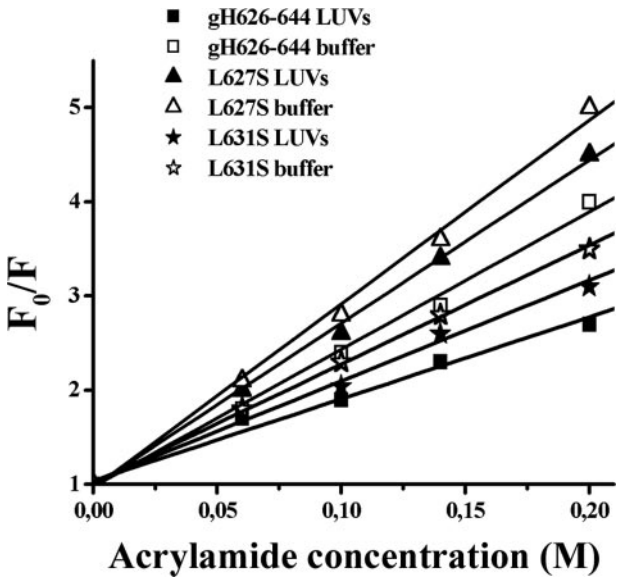

FIGURE 4. **Stern-Volmer plots of acrylamide quenching of gH-(626–644), L627S, and L631S in buffer (*open symbols*) and in LUVs (*closed symbols*).**

contain a mutation of the most N-terminal residue of gH-(626–644), this result further supports the view that gH-(626–644) enters the membrane by means of interactions at the N terminus. This result is consistent with the finding that when NBD is linked at the N terminus of this region, it enters the bilayer, whereas the tryptophan that is located in the middle of the peptide is unable to penetrate it. Peptide Y637S is unable to penetrate the bilayer, confirming the requirement for aromatic residues in membrane-penetrating peptides. Peptide W634S was not used in this experiment because the mutated residue corresponds to the tryptophan.

A lipid-exposed tryptophan residue located at the center of the hydrocarbon core of a bilayer exhibits a characteristic highly blue shifted emission, with a λ_{max} in the range of 315–318 nm (54). As a tryptophan residue moves toward the more polar membrane surface, λ_{max} gradually shifts to 335–340 nm (54–56). A smaller red shift of the fluorescence for a tryptophan at the bilayer center can also be detected upon helix oligomerization (55). This shift presumably reflects the change in local environment upon replacement of contacts between tryptophan and lipid with contacts between tryptophan and polypeptide. Our data support the hypothesis that the tryptophan is located close to the polar membrane surface and moreover that oligomerization processes may take place.

Quenching of Tryptophan by Acrylamide—The observed changes in the characteristics of the tryptophan emission upon binding of peptides gH-(626–644), L627S, and L631S to lipid vesicles indicate their insertion into the hydrophobic region of the bilayers, with the peptide gH-(626–644) showing the greatest changes in the spectra. To investigate the localization in the membrane, a quencher of tryptophan fluorescence, acrylamide, which is predominantly located in aqueous solution, was used. The more deeply a tryptophan residue is buried, the less strongly it is quenched by acrylamide. Stern-Volmer plots for the quenching of tryptophan by acrylamide, recorded in the absence and presence of lipid vesicles, are depicted in Fig. 4. Fluorescence of tryptophan decreased in a concentration-de-

TABLE 2
Stern-Volmer (K_{sv}) quenching constant calculated from the equation $F_0/F = 1 + K_{sv}[Q]$ for gH-(626–644), L627S, and L631S

	K_{sv} (M^{-1}) in buffer	K_{sv} (M^{-1}) in LUVs
gH-(626–644)	14.59	8.68
L627S	19.51	17.31
L631S	12.61	10.68

pendent manner by the addition of acrylamide to the peptide solution both in the absence and presence of liposomes, without other effects on the spectra (data not shown). However, in the presence of liposomes, less decrement in fluorescence intensity was evident, thus revealing that tryptophan is less accessible to the quencher in the presence of LUVs. The values for K_{sv} were lower for gH-(626–644) (Table 2) in LUVs, suggesting that tryptophan was more buried in the bilayers, becoming more inaccessible for quenching by acrylamide. Comparison of the plots (Fig. 4) and of the values of K_{sv} (Table 2) for the three peptides confirms that the tryptophan in gH-(626–644) is more deeply inserted than in the other two mutants; the data further support the hypothesis that the tryptophan is located close to the phospholipid heads.

Characterization of Binding Isotherms and Determination of Partition Constants—The increase in fluorescence for NBD or tryptophan binding to membrane phospholipids was used for the generation of binding isotherms for gH-(626–644) and analogues, from which partition coefficients could be calculated. The concentrations of peptides used were low enough to cause minimal aggregation in the aqueous phase and were assumed not to disrupt the bilayer structure. SUV vesicles were used in the assay to minimize light scattering effects. A control experiment was performed by titrating unlabeled peptides with lipids up to the maximal concentration used in the assay. The fluorescence intensity of this solution remained unchanged.

To determine the surface partition coefficient, the fluorescence intensities were converted to moles of bound peptide per mol of lipid and plotted as a function of the free peptide concentration as described under "Experimental Procedures." As partition coefficients depend on the concentration of lipid accessible to peptide, the curves obtained by plotting X_b* (the molar ratio of bound peptide per 60% of the total lipid) *versus* C_f (the equilibrium concentration of free peptide in the solution) are referred to as the conventional binding isotherms. The shape of a binding isotherm of a peptide can provide information on the organization of the peptide within the membrane. A straight line indicates a simple adhesion process. The shape of the binding isotherm of all the peptides tested was not linear indicating that peptide accumulation at the surface is not a simple phenomenon without cooperative association. In particular, this behavior is the hallmark for peptides that self-associate at membrane surfaces upon partitioning. If aggregation occurred only in the water but not in the bilayer phase, the opposite course of the isotherms should be expected as follows: a steep rise at the origin, followed by pronounced flattening; thus, the shape of the isotherms could be interpreted as reflecting a process whereby peptides first incorporate into the membrane and then aggregate within. Moreover, there was no evidence of aggregation in water at the concentration used in this experiment (0.1 μM); some indication of aggregation was observed at higher concentrations from native PAGE and circular dichroism studies (57). In our isotherms, the total extent of incorporation (X_b*) slowly increases until a critical concentration is reached, where massive internal aggregation apparently starts to develop.

The surface partition coefficients K_p were estimated by extrapolating the initial slopes of the curves to C_f values of zero; curves obtained for NBD-labeled peptides (gH-(626–644), R642S, and Y637S) are shown in Fig. 5, *A, C,* and *E*, whereas curves obtained for tryptophan are shown in Fig. 5, *B, D,* and *F*.

The K_p values for NBD-labeled peptides are presented in Table 3. Because K_p values are all of the same order (10^4), we concluded that the peptides have similar membrane-binding affinities. The values of K_p obtained are within the range of those obtained for membrane-permeating bioactive peptides such as melittin and its derivatives (58), the *Staphylococcus* δ-toxin (59), the antibiotic dermaseptin (60), and pardaxin analogues (36). The highest value of K_p was obtained for the native gH-(626–644) peptide, indicating that it has the highest lipid-binding affinity. All the mutations reduced the affinity even though the reduction was not drastic for any mutant peptide, indicating that the peptides penetrate the bilayer with the N terminus.

The K_p values for tryptophan-containing peptides gH-(626–644), R642S, and Y637S are shown in Table 4. The K_p value obtained for gH-(626–644) is still high (10^4), indicating that the tryptophan in gH-(626–644) is embedded in the bilayer and thus that most of the peptide gH-(626–644) is located inside the liposomes. On the contrary, the other two peptides show K_p values of 10^3 indicating that the tryptophan residue is located on the surface of the liposomes.

Secondary Structure of Synthetic Peptides—Because the structural conformation of fusion peptides has been shown to relate to fusogenic activity, the secondary structure of the peptides was determined by CD spectroscopy as measured in water and TFE. In all conditions tested, the spectra were not reliable below 200 nm because of light scattering and therefore are not shown. The CD spectra in buffer indicate that all peptides adopt a random coil conformation. A decrease in environmental polarity occurs when the peptide is transferred from water to membrane interfaces; the effect of polarity on peptide conformation can be studied using aqueous mixtures of TFE (Fig. 6). In the presence of 20% TFE, only peptide L631S shows a spectrum indicative of an extended structure, with a minimum at ~218 nm; all the other peptides gave CD spectra that suggest they have the potential to form an α-helical structure in low concentrations of TFE. However, their spectra were consistent with the peptides becoming more structured in low polarity solvent as increasing amounts of TFE induced stabilization of α-helical structures. We previously reported (20) that the peptide gH-(626–644) changed from a random coil to an α-helix upon membrane binding, and in fact the spectrum in SDS was typical of a helix. We now compared the spectrum of the native sequence in SDS with those of the mutant peptides. All the peptides showed a tendency to assume a helical structure but all

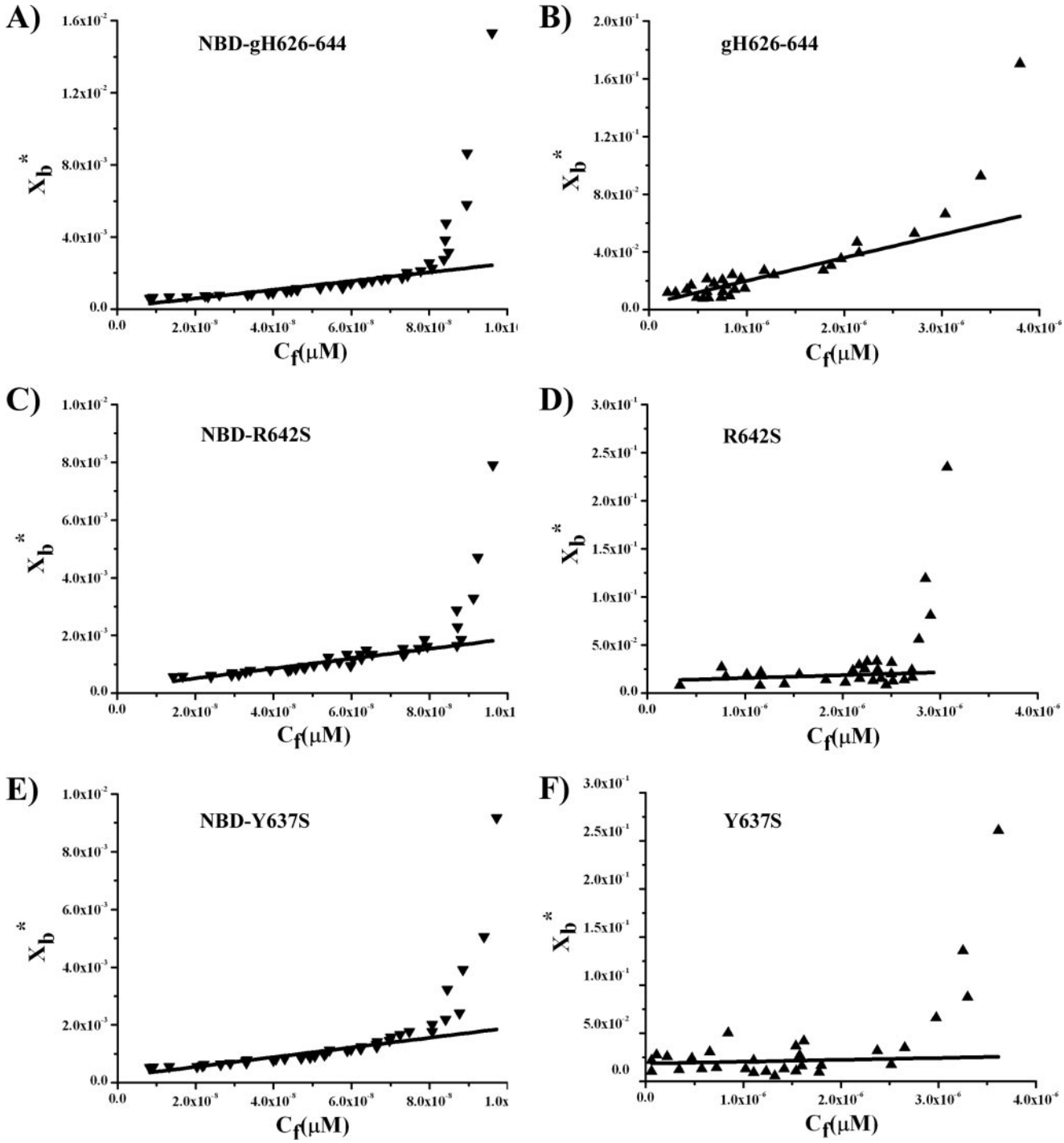

FIGURE 5. **Binding isotherms obtained plotting X_b* *versus* C_f for NBD-gH-(626–644), NBD-R642S, and NBD-Y637S (*A, C,* and *E*); binding isotherms obtained plotting X_b* *versus* C_f for gH-(626–644), R642S, and Y637S (*B, D,* and *F*).**

TABLE 3
Partition coefficient for the binding of NBD-labeled peptides with PC/Chol

	gH-(626–644)	G626S	G626V	L627S	L631S	W634S	Y637S	R642S
K_p (M^{-1})	2.42×10^4	1.8×10^4	1.79×10^4	1.97×10^4	1.64×10^4	1.7×10^4	1.7×10^4	1.7×10^4

TABLE 4
Partition coefficient for the binding of tryptophan containing peptides with PC/Chol

	gH-(626–644)	Y637S	R642S
K_p (M^{-1})	1.60×10^4	1.7×10^3	2.9×10^3

with a lower content of helix compared with the native sequence (Fig. 7).

NMR Structure of Synthetic Peptides—Because the CD analysis indicates a random coil conformation for all peptides in aqueous solution, we solved the NMR structures of gH-(626–

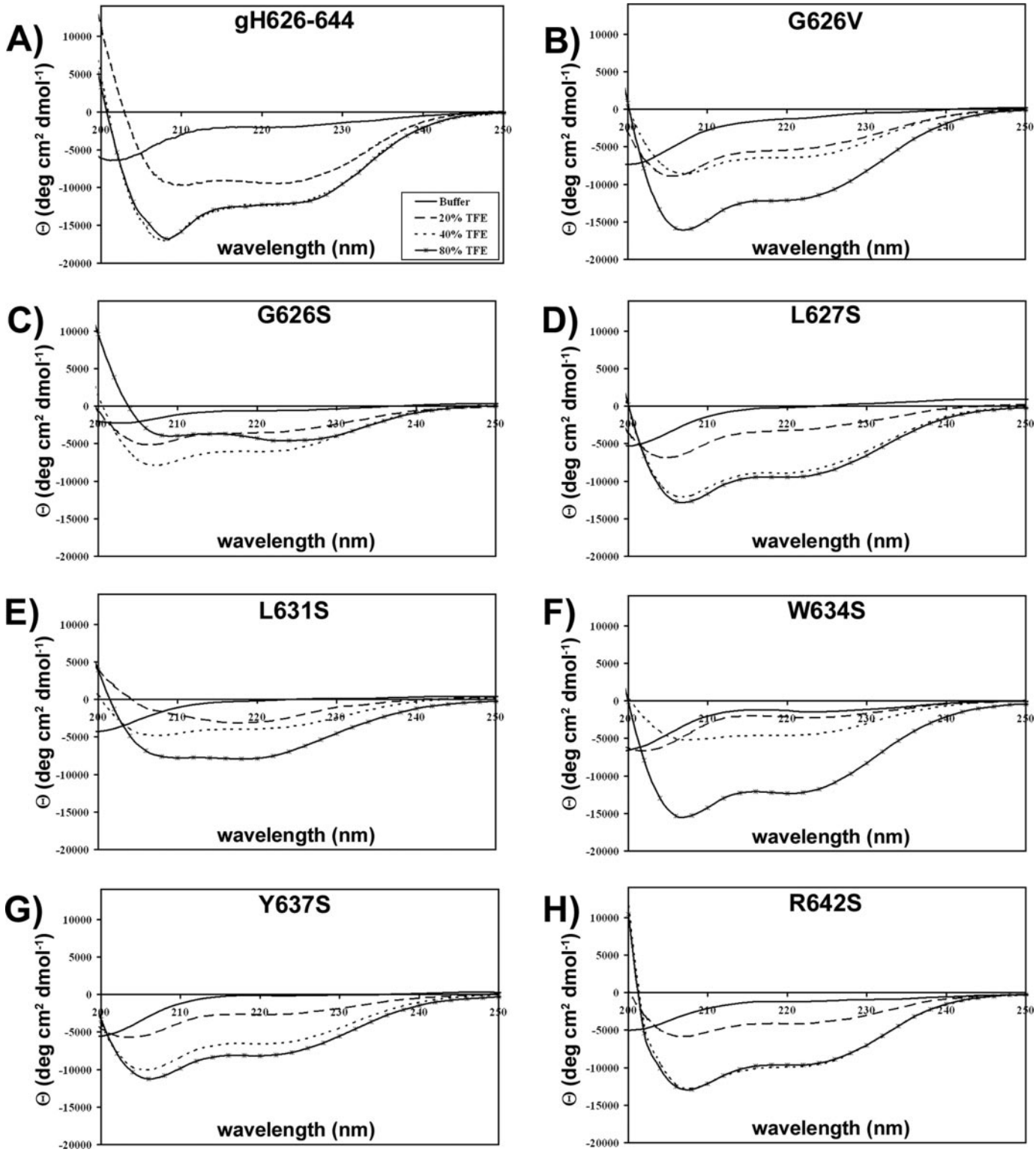

FIGURE 6. **Circular dichroism spectra of peptides at different percentages of TFE.**

644) and the two mutant peptides L627S and R642S in TFE/H_2O 80:20; the other peptides could not be analyzed by NMR because of solubility problems at the concentrations needed to perform these experiments.

^1H NMR assignments of the peptides in TFE/H_2O 80:20 were carried out by means of TOCSY, NOESY, and DQFCOSY experiments according to the standard procedures (46). Proton chemical shifts for gH-(626–644) are listed in Table 5, and all spin system proton chemical shifts of L627S and R642S are deposited in the Biological Magnetic Resonance Bank under deposition numbers 15648 and 15649, respectively. The Chemical Shift Index values, calculated following the Wishart method (61), are shown in Fig. 8 together with the NOE connectivity diagrams.

Proton-proton NOE connectivities in TFE/H_2O (80:20 v/v) were obtained from NOESY (150 ms) spectra, and a total of 184 NOEs (67 inter-residues and 117 intra-residues), 140 meaningful distance constraints, and 79 angle constraints were then used for the structure calculations of gH-(626–644). 141 NOEs (53 inter-residues and 88 intra-residues), 129 meaningful distance constraints, 78 angle constraints, 132 NOEs (47 inter-residues and 85 intra-residues), 110 meaningful distance constraints, and 78 angle constraints were obtained and used for the structure determinations of L627S and R642S, respectively. No hydrogen bonding constraints were used in the calculation. Among 100 calculated structures, the 20 with the lowest target function were selected and subjected to further minimization. All the obtained structure satisfied the NMR constraints with no NOE violations greater than 0.2 Å. The mean target functions for the 20 best conformers of gH-(626–644), L627S, and R642S were equal to 0.02, 0.10, and 0.12 $Å^2$, respectively. In Fig. 9*A*, the superimposition of the 20 lowest energy structures is reported for the gH-(626–644) fragment and its mutants. For all the calculated structures, 90% of the backbone angles ϕ and ψ fall within the allowed regions of the Ramachandran plot, and the mean values are reported in Table 6. Data concerning hydrogen bonds are reported in Table 7.

The NMR structure of gH-(626–644) (Fig. 9*B*) is well defined and consists of an α-helix conformation spanning residues 629–638 and disordered N- and C-terminal tails; the r.m.s.d. to the mean structure is 1.84 Å for the whole backbone and 0.16 Å for the Ser^{629}–Asn^{638} α-helical region. In the Ser^{629}–Asn^{638} region, seven hydrogen bonds, between the carboxylic group of the i residue and the amide group of $i + 4$ residue, stabilize the α-helical structure. Typical α-helix dihedral angle values ($\phi = -55°$ $\psi = -45°$) are found for Ser^{629}–Asn^{638} residues, whereas Leu^{627} and Ala^{628} residues show a major flexibility with average dihedral angles close to the typical α-helix conformation angles.

The overall shapes of mutants L627S and R642S resemble that of the wild type peptide with a well defined α-helix and unstructured N and C termini. However, upon close inspection subtle differences may be discerned.

Fig. 9*B* shows the NMR structure of peptide L627S. The mutation of the leucine to a serine is located in the N-terminal tail and influences the beginning of the α-helical conformation spanning in this case Thr^{630}–Asn^{638} residues. As a consequence of the substitution, residue 629 only assumes dihedral angles consistent with the α-helix structure in the 35% of the calculated structures. The average pairwise r.m.s.d. are 2.3 Å for the backbone and 0.20 Å for the folded region.

Fig. 9*B* also shows the structure of peptide R642S. The region encompassing amino acids 629–638 of this peptide assumes the same fold observed for the corresponding region in gH-(626–644) with average pairwise r.m.s.d. values of 2.37 Å for the entire backbone and 0.15 Å for the structured Ser^{629}–Asn^{638} region; also in this case, the N- and C-terminal tails appear unstructured with the R642S mutation being present in the C-terminal unstructured region.

To highlight the structural differences between the wild type and the mutant peptides, the electrostatic surface potentials are shown in Fig. 10, and this indicates the side chain orientations of all residues for the three peptides as follows: polar and charged residues are shown in *red*, hydrophobic amino acids are colored in *light gray*. The analysis of the surface of gH-(626–644) clearly shows the amphipathic nature of the wild type peptide. This amphipathic profile is clearly distinguishable in the α-helix region with a hydrophobic face constituted by Leu^{631}, Trp^{634}, Ala^{635}, and Tyr^{637} residues, and a

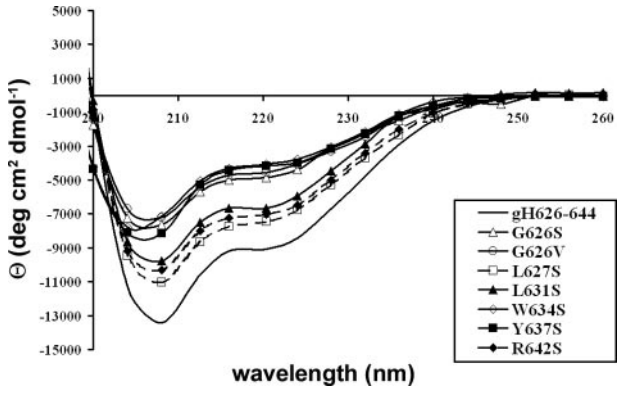

FIGURE 7. **Circular dichroism spectra of peptides in 10 mM SDS.**

TABLE 5
Proton chemical shifts (ppm) for on gH-(626–644) in TFE/H_2O (80/20, v/v) at 300 K

AA	NH	αCH	βCH	γCH	δCH	Others
Gly^{626}		4.03/3.88				
Leu^{627}	8.57	4.22	1.76	1.69	0.99	
Ala^{628}	8.29	4.18	1.51			
Ser^{629}	8.24	4.22	4.07/3.99			
Thr^{630}	7.87	4.06	4.37	1.23		
Leu^{631}	8.54	4.32	1.90	1.73	0.98/0.92	
Thr^{632}	8.09	4.11	4.34	1.34		
Arg^{633}	7.99	4.13	2.09	1.87	3.24	ϵ_{NH} 7.00
Trp^{634}	8.52	4.56	3.61/3.47			δ_1 7.19, ϵ_1 9.52, ϵ_3 7.66, ζ_2 7.47, ζ_3 7.09, η_2 7.23
Ala^{635}	8.98	3.97	1.60			
His^{636}	8.09	4.34	3.37			δ_2 8.44, ϵ_1 7.25
Tyr^{637}	8.59	4.29	3.18/3.11			δ 7.02, ϵ 6.79
Asn^{638}	8.04	4.10	2.42/2.33			δ_{22} 6.58, δ_{21} 5.02
Ala^{639}	7.66	4.08	1.47			
Leu^{640}	7.78	4.13	1.79	1.70	0.91	
Ile^{641}	7.71	3.97	1.86	1.35/1.190.79	0.75	
Arg^{642}	7.40	4.24	1.93	1.76/1.63	3.16	ϵ_{NH} 7.05
Ala^{643}	7.69	4.25	1.35			
Phe^{644}	7.60	4.68	3.24/3.10			δ 7.30, ϵ 7.24, ζ 7.24

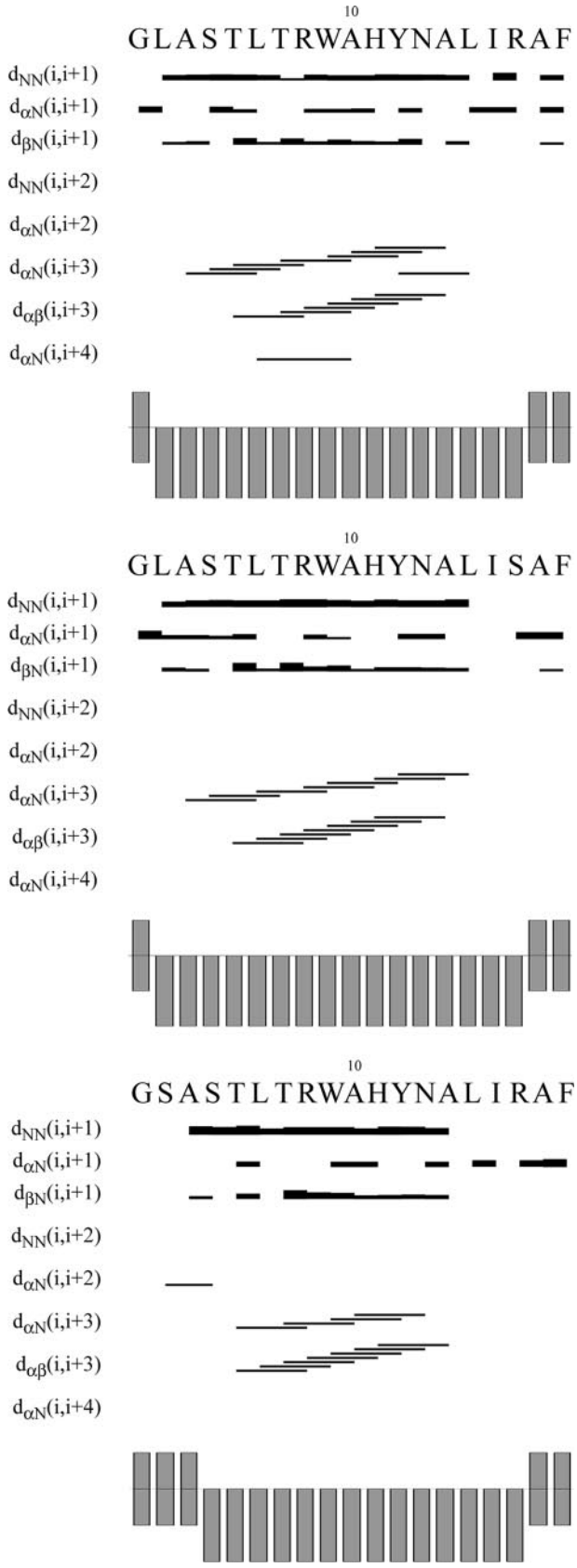

FIGURE 8. **NOE effects and CSI of gH-(626 – 644) (*upper panel*), R642S (*central panel*), and L627S (*lower panel*) in TFE/H_2O (80:20, v/v) at 300 K.**

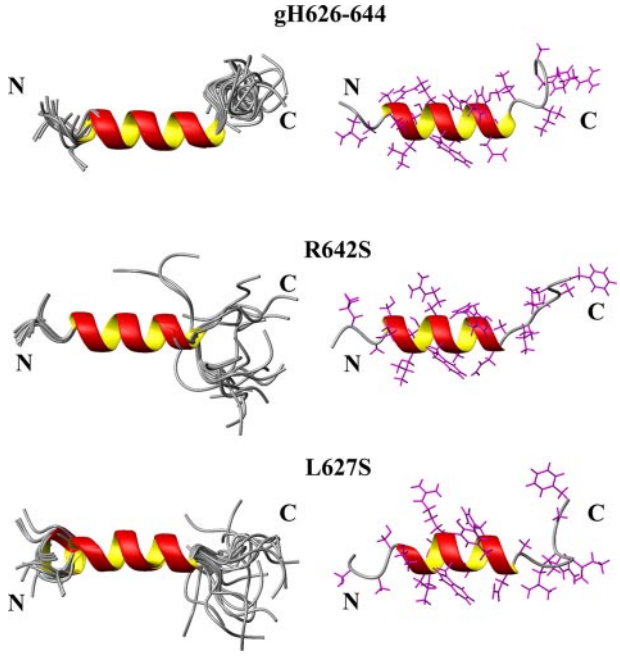

FIGURE 9. **Minimized structures of gH-(626 – 644) (*upper structure*), R642S (*central structure*), and L627S (*lower structure*) in TFE/H_2O (80:20).** *A,* superposition of the 20 best energy conformers aligned according to the minimal root mean square deviation of the backbone atoms Only the polypeptide backbone is shown. *B,* representative structures. Side chains are shown in *magenta*.

hydrophilic face constituted by Ser^{629}, Thr^{630}, Thr^{632}, Arg^{633}, and His^{636} side chains.

The amino acid substitution in L627S clearly alters the amphipathic features of the structure. In fact, the mutation results in a reduction of helical content at the N terminus. The replacement of the hydrophobic residue leucine with a polar residue serine occurs on the hydrophobic face of the helix. The amino acid substitution in R642S clearly does not influence the content of helix and the distribution of hydrophobic and hydrophilic residues because it is located in the unstructured C terminus region.

The three-dimensional structure obtained for the native peptide gH-(626 – 644) was used to predict the changes in structure that could occur as a result of substituting other residues in this region. In particular, the interaction between the aromatic ring of Trp^{634} and the side chain of Tyr^{637} seems to play a fundamental role for maintenance of the peptide interaction with the bilayer; the two residues Trp and Tyr are located on the same side of the helix and may anchor the peptide to the surface by intercalating between the lipid head groups and occupying the interfacial region (between the hydrophobic interior and the polar head groups); mutation of either amino acid clearly reduces the strength of the interaction with the bilayer as well as their fusogenic activity. The other important residue for fusogenic activity is Gly^{626}; this residue is the first at the N terminus and is already disordered in the native sequence.

Effect of Mutated gH-(626 – 644) Peptides on HSV1 Infectivity—Several reports in the literature (62–64) describe the potential of fusion peptide analogues of orthomyxoviruses, paramyxoviruses, and human immunodeficiency virus as virus entry inhibitors. The accepted view is that the infectivity inhibition may be

TABLE 6
Backbone dihedral angles (°) for gH-(626–644), R642S, and L627S averaged over the 20 NMR structures with the lowest energy

Amino acid	gH-(626–644)		R642S		L627S	
	ϕ	ψ	ϕ	ψ	ϕ	ψ
Gly^{626}		179 ± 38		−172 ± 20		−115 ± 91
Leu^{627}	−91 ± 82	−73 ± 52	−57 ± 56	−34 ± 55	−63 ± 10	130 ± 60
Ala^{628}	−51 ± 64	−35 ± 27	62 ± 3	−18 ± 11	37 ± 96	9 ± 35
Ser^{629}	−34 ± 22	−53 ± 30	−56 ± 4	−21 ± 6	−27 ± 51	−1 ± 36
Thr^{630}	−49 ± 29	−55 ± 6	−57 ± 7	−61 ± 2	−57 ± 9	−38 ± 4
Leu^{631}	−57 ± 5	−51 ± 4	−60 ± 3	−35 ± 2	−44 ± 8	−45 ± 3
Thr^{632}	−56 ± 3	−47 ± 6	−62 ± 1	−52 ± 5	−64 ± 3	−45 ± 4
Arg^{633}	−58 ± 6	−51 ± 11	−63 ± 3	−31 ± 3	−62 ± 4	−39 ± 2
Trp^{634}	−55 ± 10	−55 ± 1	−53 ± 2	−54 ± 1	−64 ± 3	−44 ± 4
Ala^{635}	−54 ± 1	−56 ± 2	−60 ± 3	−31 ± 8	−57 ± 3	−21 ± 7
His^{636}	−57 ± 3	−45 ± 6	-69 ± 6	−34 ± 5	−72 ± 4	−25 ± 5
Tyr^{637}	−59 ± 3	−53 ± 7	−61 ± 5	−43 ± 3	−64 ± 3	−48 ± 5
Asn^{638}	−56 ± 5	−43 ± 3	−70 ± 25	−16 ± 24	−62 ± 8	−58 ± 17
Ala^{639}	−72 ± 8	−17 ± 23	42 ± 68	14 ± 41	56 ± 7	−159 ± 97
Leu^{640}	39 ± 70	132 ± 29	63 ± 9	104 ± 82	179 ± 84	109 ± 38
Ile^{641}	−69 ± 23	−12 ± 56	−66 ± 10	23 ± 93	−64 ± 11	112 ± 67
Arg^{642}	−163 ± 90	−105 ± 92	−76 ± 95	102 ± 40	−34 ± 76	92 ± 24
Ala^{643}	85 ± 106	53 ± 43	−107 ± 83	140 ± 46	−148 ± 78	139 ± 30
Phe^{644}	128 ± 77		−144 ± 83		−81 ± 64	

TABLE 7
Hydrogen bond distances and angles obtained for gH-(626–644), R642S, and L627S

Donor-acceptor	gH-(626–644)		R642S		L627S	
	H-O distance	N-H···O angle	H-O distance	N-H···O angle	H-O distance	N-H···O angle
	Å	°	Å	°	Å	°
Leu^{631}(HN)-Ala^{628}(O)					1.9–2.3	10–29
Thr^{632}(HN)-Ala^{628}(O)	1.8–2.0	3–9	2.2–2.5	8–17		
Arg^{633}(HN)-Ser^{629}(O)	1.8–2.0	4–17	2.0–2.8	8–20	2.7–3.4	9–25
Trp^{634}(HN)-Thr^{630}(O)	1.8–1.9	5–11	1.9–2.3	15–28	1.6–1.8	7–18
Ala^{635}(HN)-Leu^{631}(O)	1.8–1.9	1–13	2.0–2.4	1–7	1.8–1.9	3–11
His^{636}(HN)-Thr^{632}(O)	1.8–1.9	7–11	2.3–2.9	9–45		
His^{636}(HN)-Arg^{633}(O)					2.0–2.6	24–33
Thr^{637}(HN)-Arg^{633}(O)	1.8–1.9	3–19	1.9–2.3	20–34		
Tyr^{637}(HN)-Trp^{634}(O)					1.9–2.3	15–32
Asn^{635}(HN)-Trp^{634}(O)	1.8–1.9	3–19	1.9–3.4	2–29	2.0–3.0	2–20
Ala^{639}(HN)-Ala^{635}(O)	1.8–1.9	9–19	2.3–2.7	6–34	1.9–2.3	9–30
Leu^{640}(HN)-His^{636}(O)	1.8–1.9	3–20	2.2–2.5	8–17		
Leu^{640}(HN)-Tyr^{637}(O)	1.8–1.9	13–19	2.0–2.8	8–20		

due to the formation of inactive aggregates between the fusogenic stretches present in the viral protein and the synthetic peptides. These aggregates are formed as a consequence of their intrinsic oligomerization nature and are predicted to stabilize a pre-fusion intermediate and prevent merging of the bilayers. We therefore determined whether peptides containing mutations in the region 626–644 of HSV gH were as efficient as the wild type version at inhibiting HSV infection. To verify that the peptides did not exert toxic effect on Vero cells, monolayers were exposed to different concentrations (10, 25, 50, and 100 μM) of each peptide for 24 h, and cell viability was assayed by a lactate dehydrogenase assay. No statistical difference was observed between the viability of control (untreated) cells and that of cells exposed to the peptides (data not shown).

To test whether the mutated peptides could affect HSV infectivity, Vero cells were infected with HSV at 37 °C in the presence or absence of each peptide. Plaque formation was measured 48 h post-infection. These results are shown in Fig. 11.

In a dose-dependent inhibition assay of HSV entry, we compared the activity of mutant peptides with that of the wild type gH-(626–644) and found that all mutant peptides exhibited a consistent lower extent of inhibition. Whereas 60 μM of gH-(626–644) caused 50% inhibition of infection, none of the mutated peptides was able to induce more than 20% inhibition at the same concentration.

DISCUSSION

We have studied the structure of a peptide derived from a region of HSV-1 gH encompassing amino acids 626–644 and have examined its ability to interact with membranes. We have compared the properties of a peptide containing the wild type sequence with those of peptides containing amino acid substitutions at specific residues in this region. By using mainly fluorescence methodologies to study the interaction of peptides with model membranes, we showed the following. (i) The gH-(626–644) peptide interacts with model membranes as determined by monitoring changes in fluorescence intensity and blue shifts that occur upon addition of vesicles, and these data indicate that the N terminus initially penetrates the bilayer. (ii) Quenching studies indicate that the tryptophan residue in gH-(626–644) is buried inside the bilayer, indicating that at least half of the peptide is located within the bilayer. (iii) gH-(626–644) is able to induce membrane fusion (as reported previously (20)) with an elevated plasticity that tends to adopt a stable α-helical conformation in membrane mimetic environments. (iv) The peptide, when in α-helical conformation, is also characterized by a strong

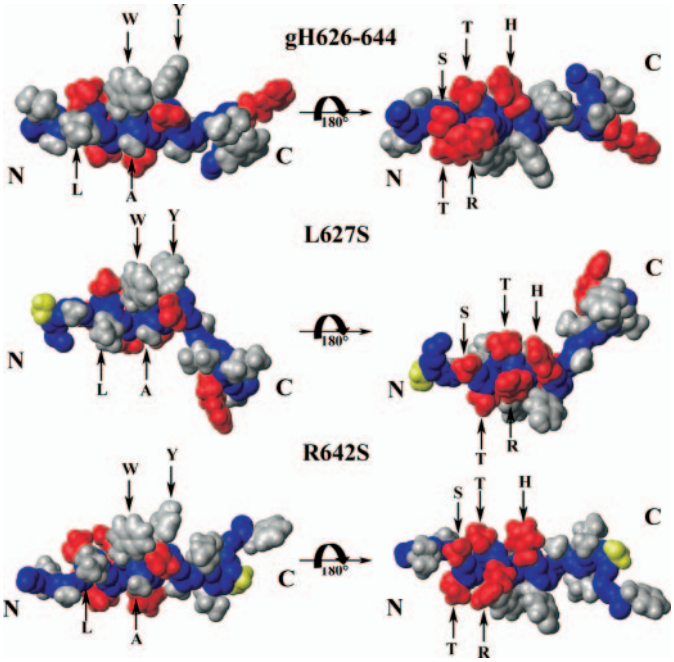

FIGURE 10. **Side-chain orientations of gH-(626–644) (*upper structure*), R642S (*central structure*), and L627S (*lower structure*) peptides.** The van der Waals surface of the representative conformer in TFE/H_2O (80:20) is shown. Polar and charged residues are shown in *red*; hydrophobic amino acids are colored in *light gray*; mutated residues in R642S and L627S peptides are colored in *yellow*.

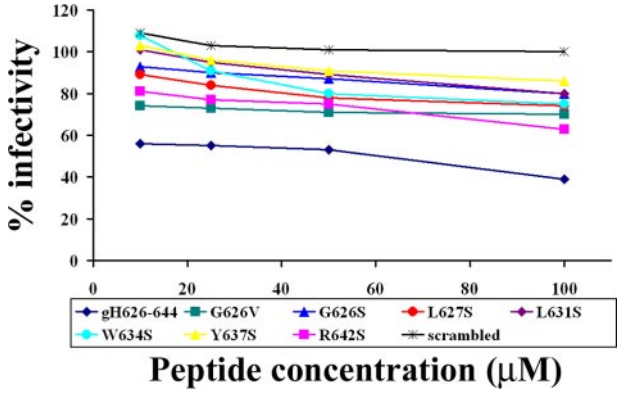

FIGURE 11. **Cells were incubated with increasing concentrations of the peptides (10, 25, 50, and 100 μM) in the presence of the viral inoculum for 45 min at 37 °C.** Nonpenetrated virus was inactivated, and cells were incubated for 48 h at 37 °C in DMEM supplemented with carboxymethylcellulose. Plaque numbers were scored, and the percentage of inhibition was calculated with respect to no-peptide control experiments. Data are reported in triplicate, and *error bars* represent S.D.

amphipathic propensity. (v) A peptide comprising residues 626–644 of gH inhibits HSV infection.

To our knowledge, this is the first detailed molecular and biophysical characterization of an HSV-1 gH fusogenic region. Moreover, these data also confirm the functional importance of this sequence because peptides with single amino acid substitutions of several residues in this region were less active in fusion experiments. The results of the mutagenic analysis are consistent with the observation that mutations affecting fusion proteins of other viruses affect infectivity, and mutations in the sequences of the corresponding synthetic peptides are less efficient at fusing liposomes. Such hydrophobic peptides are predicted to insert into lipid bilayers, causing local membrane destabilization and initiating the fusion of host and viral membranes. The peptide gH-(626–644) contains particular residues that are crucial for the capacity of the peptide to interact and destabilize target lipid membranes. It is rich in hydrophobic residues, including glycines, leucines, alanines, and aromatic residues such as tryptophan and tyrosines; aromatic residues are known to preferentially interact at the membrane interface. The region contains only a few charged residues. The functional role of each residue in membrane fusion was assessed using mutated peptides in which specific amino acids were substituted by serine; the aim was to assess the impact of these substitutions on membrane interaction capability and to analyze any differences in the three-dimensional structure.

All gH-(626–644) mutated peptides showed a reduced ability to induce fusion, as well as reduced penetration into the bilayer. In fact, with the exception of the two peptides containing substitutions of leucine residues (L627S and L631S), which in the tryptophan quenching experiment gave results comparable with the wild type gH-(626–644), the other mutated peptides showed a lower degree of penetration, but all of them, including the two leucine mutants, were still available to enzymatic digestion, and are therefore presumably less well embedded in model membranes.

Amphipathic helices are commonly believed to play a crucial role for mediating lipid-protein interactions during the binding of proteins to membranes. Once bound, the hydrophobic face of the amphipathic peptide would then permit the peptide to enter the membrane interior, thereby triggering local fusion of the membrane leaflets, pore formation, cracks, and membrane fusion. Viral fusion peptides are believed to assume an amphipathic α-helix structure once they become bound to membranes. They undergo conformational changes when they reach the target membrane, which enables them to associate with the membrane and fuse them. An amphipathic α-helix is believed to be an important feature of fusion peptides, and indeed CD and NMR data reveal the highly amphipathic nature of gH-(626–644) with its hydrophobic residues on one face of the helix and polar or charged residues on the opposite face.

The interaction of the fusion peptide with the cell membrane is essential for viral and cell membrane fusion to take place, and here we have shown that mutations in the sequence of the HSV-1 gH membrane-interacting region that reduce its hydrophobicity severely affect the fusion activity. The ability of native and mutant peptides to interact with membranes was determined from fluorescence studies of either intrinsic tryptophan residues or NBD groups attached at the N terminus of each peptide in the presence of model membranes. The fluorescence intensity of the peptides increased upon increasing the lipid/peptide ratio, indicating a significant change in the environment of the tryptophan or of the NBD moieties of the peptides; the changes of fluorescence allowed us to obtain partition coefficients (K_p). K_p values in the range 10^4 were obtained for the NBD moieties of all the peptides (although the highest value was obtained for the native peptide), indicating that all the peptides penetrate with their N terminus inside the membrane. K_p values of 10^4 were obtained for the tryptophan fluorescence changes of the native peptide only indicating that its tryptophan

(in the middle of the peptide) is located inside the membrane; on the contrary the K_p values for all the mutant peptides still showing a modification of the tryptophan spectrum were in the range 10^3 indicating a less strong interaction with the membrane and thus probably a different location on the surface of the membrane. These results may indicate that only the native peptide penetrates strongly inside the membrane, whereas all the mutant peptides are less able to penetrate and are partially outside the membrane, thus explaining their lower activity in fusion assays.

The results obtained with peptides containing substitution of glycine 626 (G626S and G626V) are of further note because many fusogenic regions contain highly conserved glycine residues, and their mutation can impair or completely eliminate the fusion activity of fusion proteins. Several mutagenesis studies indicate that the glycine at the N terminus of influenza virus HA2 fusion peptide is particularly critical, and substitution of this residue with more polar or more hydrophobic residues results in a complete loss of activity; the only tolerated change in this position appears to be an alanine. A particularly interesting mutant is G1S of HA2, because replacing the glycine with a serine facilitates lipid mixing but not content mixing (65, 66). Also the ability of human immunodeficiency virus type 1 gp41 to promote membrane fusion can be completely abolished by a single mutation G10V within the fusion peptide (67). Our results seem to confirm this view that glycine residues in membrane-interacting peptides are functionally important for the fusion process. Our results indicate that peptides G626S and G626V are both severely impaired in their ability to fuse membranes, with the G626S mutant having a more drastic effect. As proposed by Li *et al.* (65), the requirement for a glycine at the N terminus of membrane-interacting peptides may be a general motif; the glycine may be the ideal interface on a membrane-inserted helix to interact with other helices in membranes. The actually accepted scenario supports the hypothesis that several membrane interacting domains in HSV gH are involved in the fusion of viral and cellular membranes, and thus intra- or intermolecular interactions between fusion domains may occur through the glycine edge of the N-terminal arm of gH-(626–644) and some unidentified residues of the other membrane interacting sequences. In the three-dimensional structure (as determined by NMR) the glycine residue is the first residue at the N terminus, thus the NMR studies did not provide a structural explanation for the loss of activity.

Mutants L627S and L631S are slightly less active in fusion assays, suggesting that leucines may also be crucial for the proper positioning of the peptides in membranes. The results obtained from NMR studies are particularly interesting; in fact, the most striking effect of the mutation L627S is a clear loss of the amphipathic character, confirming that the amphipathic nature of this region is also important for fusion.

The important role of tryptophan and tyrosine in gH-(626–644) (as highlighted from studies of peptides W^{634} and Y637S) is consistent with the known preference of these amino acids for the interfacial lipid head groups. In particular, the planar indole ring of tryptophan is thought to favor interfacial localization because of several factors as follows: a hydrophobic effect that would drive it out of the aqueous solvent, complex electrostatic interactions that favor its location within the hydrated head group region, and repulsive forces that keep it out of the hydrocarbon core. Interestingly, the importance of tryptophan residues in membrane interacting domains also seems to be shared by β-barrel membrane bacterial proteins; thus, the interfacial interaction of one or more tryptophan residues with the membrane appears to be a common property of membrane interacting domains from quite evolutionarily divergent proteins (68, 69). Both the tryptophan and tyrosine appear to be on the same side of the helix in the three-dimensional structure of gH-(626–644), forming an amphiphilic helix in which one side is constituted by aromatic and hydrophobic residues, whereas the other side is formed by hydrophilic or small residues. Mutation of these two amino acids led to a reduced ability of such peptides to fuse membranes, and even though the α-helical character is maintained, the peptides penetrate less into in the membrane. Unfortunately, changes in structure could not be analyzed by NMR because of their poor solubility.

Recently, Freitas *et al.* (70) reported the structure of the Ebola fusion peptide in a membrane-mimetic environment. The Ebola fusion peptide contains the same motif as gH-(626–644), with a tryptophan and a tyrosine separated by two non-aromatic residues, and suggested the strong importance of the tryptophan and tyrosine for structure maintenance within the membrane bilayer. In particular, it has been hypothesized that the interaction between the aromatic ring of tryptophan and the side chain of tyrosine is important for maintenance of structural stability during the interaction with the membrane; we found a similar interaction in gH-(626–644).

The critical role played by tryptophan and tyrosine in fusion peptides was also demonstrated for influenza virus (71, 72); the structure of the fusion peptide was determined by NMR in micelles; the domain is a kinked predominantly helical amphipathic structure. The kinked structure is stabilized by two hydrophobic clusters consisting of a phenylalanine and an isoleucine on the N-terminal side and a tryptophan on the C-terminal side of the kink. Both are necessary and sufficient to anchor the fusion domain in the proper conformation in the interface of the lipid bilayer. Thus, our data further support the importance of aromatic residues for fusion activity, and their presence may represent a common feature of fusion peptides.

Our results suggest that differences in membrane binding and lipid mixing are also strongly dependent on the presence of a positive charge at the C terminus of the fusion peptide; the arginine localized at the C terminus is probably involved in interactions with the polar head groups, and we found that R642S is severely compromised in its fusion activity. The mutation renders the peptide unable to penetrate into the bilayer, and as a consequence the affinity constants for the bilayer are much lower. The mutant peptide R642S is also particularly intriguing because it is now commonly believed that arginines play an important role inside the fusion peptides and may represent an important factor in defining the molecular mechanism by which the virus enters the target cell (73). We have also determined the structure of R642S by NMR, but because this residue is localized in an unstructured region of the peptide, it

was not possible to determine the impact of this substitution on structural features of this region.

Finally, a further indication of the importance of this region of HSV gH is the fact that all peptides tested with mutations in this stretch of amino acids were less efficient than the wild type peptide at inhibiting HSV infection. Taken together, these data raise the possibility that gH might operate during fusion by actively using the sequence gH-(626–644) to perturb the lipid bilayer of apposing membranes and that its content of ellipticity and aromatic residues is of fundamental importance.

REFERENCES

1. Rey, F. A. (2006) *EMBO Rep.* **7,** 1000–1005
2. Shukla, D., and Spear, P. G. (2001) *J. Clin. Investig.* **108,** 503–510
3. Montgomery, R. I., Warner, M. S., Lum, B. J., and Spear, P. G. (1996) *Cell* **87,** 427–436
4. Geraghty, R. J., Krummenacher, C., Cohen, G. H., Eisenberg, R. J., and Spear, P. G. (1998) *Science* **280,** 1618–1620
5. Warner, M. S., Geraghty, R. J., Martinez, W. M., Montgomery, R. I., Whitbeck, J. C., Xu, R., Eisenberg, R. J., Cohen, G. H., and Spear, P. G. (1998) *Virology* **246,** 179–189
6. Shukla, D., Liu, J., Blaiklock, P., Shworak, N. W., Bai, X., Esko, J. D., Cohen, G. H., Eisenberg, R. J., Rosenberg, R. D., and Spear, P. G. (1999) *Cell* **99,** 13–22
7. Carfí, A., Willis, S. H., Whitbeck, J. C., Krummenacher, C., Cohen, G. H., Eisenberg, R. J., and Wiley, D. C. (2001) *Mol. Cell* **8,** 169–179
8. Fusco, D., Forghieri, C., and Campadelli-Fiume, G. (2005) *Proc. Natl. Acad. Sci. U. S. A.* **102,** 9323–9328
9. Heldwein, E. E., Lou, H., Bender, F. C., Cohen, G. H., Eisenberg, R. J., and Harrison, S. C. (2006) *Science* **313,** 217–220
10. Krummenacher, C., Supekar, V. M., Whitbeck, J. C, Lazear, E., Connolly, S. A., Eisenberg, R. J., Cohen, G., Wiley, D. C., and Carfi, A. (2005) *EMBO J.* **24,** 4144–4153
11. Spear, P. G., Manoj, S., Yoon, M., Jogger, C. R., Zago, A., and Myscofski, D. (2006) *Virology* **344,** 17–24
12. Satoh, T., Arii, J., Suenaga, T., Wang, J., Kogure, A., Uehori, J., Arase, N., Shiratori, I., Tanaka, S., Kawaguchi, Y., Spear, P. G., Lanier, L. L., and Arase, H. (2008) *Cell* **132,** 935–944
13. Forrester, A., Farrell, H., Wilkinson, G., Kaye, J., Davis-Poynter, N., and Minson, T. (1992) *J. Virol.* **66,** 341–348
14. Turner, A., Bruun, B., Minson, T., and Browne, H. (1998) *J. Virol.* **72,** 873–887
15. Kielian, M., and Rey, F. A. (2006) *Nat. Rev. Microbiol.* **4,** 67–76
16. Gage, P. J., Levine, M., and Glorioso, J. C. (1993) *J. Virol.* **67,** 2191–2201
17. Galdiero, S., Vitiello, M., D'Isanto, M., Falanga, A., Cantisani, M., Browne, H., Pedone, C., and Galdiero, M. (2008) *ChemBioChem* **9,** 758–767
18. Weissenhorn, W., Hinz, A., and Gaudin, Y. (2007) *FEBS Lett.* **581,** 2150–2155
19. Roche, S., Bressanelli, S., Rey, F. A., and Gaudin, Y. (2006) *Science* **313,** 187–191
20. Galdiero, S., Falanga, A., Vitiello, M., Browne, H., Pedone, C., and Galdiero, M. (2005) *J. Biol. Chem.* **280,** 28632–28643
21. Gianni, T., Martelli, P. L., Casadio, R., and Campadelli-Fiume, G., (2005) *J. Virol.* **79,** 2931–2940
22. Cairns, T. M., Landsburg, D. J., Whitbeck, J. C., Eisenberg, R. J., and Cohen, G. H. (2005) *Virology* **332,** 550–562
23. Cairns, T. M., Milne, R. S. B., Ponce-de-Leon, M., Tobin, D. K., Cohen, G. H., and Eisenberg, R. J. (2003) *J. Virol.* **77,** 6731–6742
24. Galdiero, M., Whiteley, A., Bruun, B., Bell, S., Minson, T., and Browne, H. (1997) *J. Virol.* **71,** 2163–2170
25. Hutchinson, L., Browne, H., Wargent, V., Davis-Poynter, N., Primorac, S., Goldsmith, K., Minson, A. C., and Johnson D. C. (1992) *J. Virol.* **66,** 2240–2250
26. Roop, C., Hutchinson, L., and Johnson, D. C. (1993) *J. Virol.* **67,** 2285–2297
27. Harman, A., Browne, H., and Minson, T. (2002) *J. Virol.* **76,** 10708–10716
28. Wilson, D. W., Davis-Poynter, N., and Minson, A. C. (1994) *J. Virol.* **68,** 6985–6993
29. Galdiero, S., Vitiello, M., D'Isanto, M., Falanga, A., Collins, C., Raieta, K., Pedone, C., Browne, H., and Galdiero, M. (2006) *J. Gen. Virol.* **87,** 1085–1097
30. Gianni, T., Menotti, L., and Campadelli-Fiume, G. (2005) *J. Virol.* **79,** 7042–7049
31. Lopper, M., Compton, T. (2004) *J. Virol.* **78,** 8333–8341
32. Galdiero, S., Falanga, A., Vitiello, M., D'Isanto, M., Collins, C., Orrei, V., Browne, H., Pedone, C., and Galdiero, M. (2007) *ChemBioChem.* **8,** 885–895
33. Subramanian, R. P., and Geraghty, R. J. (2007) *Proc. Natl. Acad. Sci. U. S. A.* **104,** 2903–2908
34. Atanasiu, D., Whitbeck, J. C., Cairns, T. M., Reilly, B., Cohen, G. H., and Eisenberg, R. J. (2007) *Proc. Natl. Acad. Sci. U. S. A.* **104,** 18718–18723
35. Wimley, W. C., and White, S. H. (1996) *Nat. Struct. Biol.* **3,** 842–848
36. Rapaport, D., and Shai, Y. (1991) *J. Biol. Chem.* **266,** 23769–23775
37. Struck, D. K., Hoekstra, D., and Pagano, R. E. (1981) *Biochemistry* **20,** 4093–4099
38. Mao, D., and Wallace, B. A. (1984) *Biochemistry* **23,** 2667–2673
39. Schwarz, G., Stankowsky, S., and Rizzo, V. (1986) *Biochim. Biophys. Acta* **861,** 141–151
40. Beschiaschvili, G., and Seeling, J. (1990) *Biochemistry* **29,** 52–58
41. De Kroon, A. I. P. M., Soekarjo, M. W., De Gier, J., and De Kruijff, B. (1990) *Biochemistry* **29,** 8229–8240
42. Eftink, M. R., and Ghiron, C. A. (1976) *J. Phys. Chem.* **80,** 486–493
43. Killian, J. A., Trouard, T. P., Greathouse, D. V., Chupin, V., and Lindblom, G. (1994) *FEBS Lett.* **348,** 161–165
44. Bartels, C., Xia, T., Billeter, M., and Wüthrich, K. (1995) *J. Biomol. NMR* **5,** 1–10
45. Hwang, T. L., and Shaka, A. J. (1995). *J. Magn. Reson. A* **112,** 275–279
46. Cavanagh, J., Fairbrother, W. J., Palmer, A. G., and Skelton, N. J. (1996) *Protein NMR Spectroscopy: Principles and Practice*, Academic Press, Inc., San Diego
47. Herman, T., Guntert, P., and Wüthrich., K. (2002) *J. Mol. Biol.* **319,** 209–227
48. Koradi, R., Billeter, M., and Wüthrich, K. (1996) *J. Mol. Graphics* **14,** 51–55
49. Gazit, E., Boman, A., Boman, H. G., and Shai, Y. (1995) *Biochemistry* **34,** 11479–11488
50. Rajarathnam, K., Hochman, J., Schindler, M., and Ferguson-Miller, S. (1989) *Biochemistry* **31,** 3168–3176
51. Rapaport, D., and Shai, Y. (1992) *J. Biol. Chem.* **267,** 6502–6509
52. Pouny, Y., and Shai, Y. (1992) *Biochemistry* **31,** 9482–9490
53. Yau, W. M., Wimley, W. C., Gawrisch, K., and White, S. H. (1998) *Biochemistry* **37,** 14713–14718
54. Ren, J., Lew, S., Wang, Z., and London, E. (1997) *Biochemistry* **36,** 10213–10220
55. Ren, J., Lew, S., Wang, J., and London, E. (1999) *Biochemistry* **38,** 5905–5912
56. Hammond, K., Caputo, G. A., and London, E. (2002) *Biochemistry* **41,** 3243–3253
57. Galdiero, S., Vitiello, M., Falanga, A., D'Isanto, M., Cantisani, M., Kampanaraki, A., Benedetti, E., Browne, H., and Galdiero, M. (2008) *Peptides* **9,** 1461–1471
58. Stankowski, S., and Schwarz, G. (1990) *Biochim. Biophys. Acta* **1025,** 164–172
59. Thiaudière, E., Siffert, O., Talbot, J. C., Bolard, J., Alouf, J. E., and Dufourcq, J. (1991) *Eur. J. Biochem.* **195,** 203–213
60. Pouny, Y., Rapaport, D., Mor, A., Nicolas, P., and Shai, Y. (1992) *Biochemistry* **31,** 12416–12423
61. Wishart, D. S., Sykes, B. D., and Richards, F. M. (1992) *Biochemistry* **31,** 1647–1651
62. Richardson, C. D., Scheid, A., and Choppin, P. W. (1980) *Virology* **105,** 205–222
63. Kliger, Y., Aharoni, A., Rapaport, D., Jones, P., Blumenthal, R., and Shai, Y. (1997) *J. Biol. Chem.* **272,** 13496–13505
64. Silburn, K. A., McPhee, D. A., Maerz, A. L., Poumbourios, P., Whittaker, R. G., Kirkpatrick, A., Reilly, W. G., Manthey, M. K., and Curtain, C. C.

(1998) *AIDS Res. Hum. Retrovirus* **14,** 385–392
65. Li, Y., Han, X., Lai, A. L., Bushweller, J. H., Cafiso, D. S., and Tamm, L. K. (2005) *J. Virol.* **79,** 12065–12076
66. Qiao, H., Armstrong, R. T., Melikyan, G. B., Cohen, F. S., and White, J. M. (1999) *Mol. Biol. Cell* **10,** 2759–2769
67. Delahunty, M. D., Rhee, I., Freed, E. O., and Bonifacino, J. S. (1996) *Virology* **218,** 94–102
68. Galdiero, S., and Gouaux, E. (2004) *Protein Sci.* **13,** 1503–1511
69. Galdiero, S., Galdiero, M., and Pedone, C. (2007) *Curr. Protein Pept. Sci.* **8,** 63–82
70. Freitas, M. S., Gaspar, L. P., Lorenzoni, M., Almeida, F. C. L., Tinoco, L. W., Almeida, M. S., Maia, L. F., Degréve, L., Valente, A. P., and Silva J. L. (2007) *J. Biol. Chem.* **282,** 27306–27314
71. Han X., Bushweller, J. H., Cafiso D. S., and Tamm, L. K. (2001) *Nat. Struct. Biol.* **8,** 715–720
72. Lai, A. L., and Tamm, L. K. (2007), *J. Biol. Chem.* **282,** 23946–23956
73. Buzon, V., Padros, E., and Cladera, J. (2005) *Biochemistry* **44,** 13354–13364